Investigating the origins of the 'double rise' shape in hydrogen permeation transients on pure iron,

Sarah Alzein, Alixe Dreano, Frédéric Christien

Corrosion Science 231 (2024) 111998

Contents lists available at ScienceDirect

Corrosion Science

journal homepage: www.elsevier.com/locate/corsci

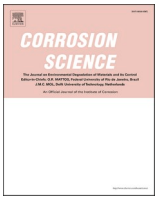

Investigating the origins of the 'double rise' shape in hydrogen permeation transients on pure iron

Sarah Alzein *, Alixe Dreano, Frederic Christien

Mines Saint-Etienne, Univ Lyon, CNRS, UMR 5307 LGF, Saint-Etienne F-42023, France

ARTICLE INFO

Keywords:
Electrochemical permeation
FEM model
Micro-porosity
Diffusion
Hydrogen damage

ABSTRACT

This study delves into the underlying causes of the atypical 'double rise' shape observed in hydrogen permeation rising transients on pure iron and low alloy steels. Electrochemical permeation experiments on pure iron reveal a fast initial rise, a short pseudo-plateau, and a slow second rise. Similar patterns emerge in the decaying transients. The micro-porosity present in material appears to act as reversible traps, affecting hydrogen diffusion. Surface damage, confirmed by SEM analysis, exacerbates the issue. Utilizing numerical simulations, an FEM model effectively replicates the 'double rise' behavior, attributed to limited recombination/dissociation kinetics at bulk-cavity interfaces. Overall, micro-porosity is identified as the primary factor behind this unique permeation curve shape.

1. Introduction

As the world pivots towards cleaner, carbon-free energy sources, hydrogen has emerged as a potential key player to address the escalating demand for sustainable energy solutions. However, the utilization of hydrogen as a viable energy source requires meticulous consideration of its interactions with materials employed in hydrogen storage, transportation, and other related applications. A critical concern in this pursuit revolves around the impact of hydrogen on the durability of metals in hydrogen-rich environments [1]. Significant research efforts were dedicated to developing materials with specific properties for various applications such as high strength steels. However, a notable obstacle arises: many of these materials could not be used because they are prone to hydrogen embrittlement, which is the deterioration of mechanical properties due to the presence of dissolved hydrogen in the metals [2]. Hydrogen diffuses into the metal lattice interstitially through the metal surface. As it diffuses through the lattice, it interacts with various traps including porosities, grain boundaries, precipitates, dislocations, and others [3–5]. Gaining an understanding of the mechanisms of hydrogen-metal interactions is essential for designing materials capable of resisting hydrogen embrittlement.

Despite its sensitivity and difficulties of obtaining reproducible results, the electrochemical hydrogen permeation experiment stands as one of the foremost and widely used techniques for characterizing hydrogen diffusion in metals [6–13]. In this regard, several studies yielded atypical permeation results that persist consistently across different materials -mainly pure iron and low alloy steels- and conditions, sparking disagreement among researchers regarding the underlying causes of such abnormal hydrogen permeation behavior [6,8,10–12]. This anomalous permeation behavior is characterized by a consistent profile: an initial first rise in hydrogen until reaching a pseudo-steady state which is followed by a slight drop in some cases. Subsequently, a significant second rise in hydrogen permeation ensues, followed by another steady state region and a possible slight decrease. A few studies have attempted to tackle the reasons causing this abnormal 'double-rise' shape [6,8,10,11,13] with some authors attributing it to surface effect while others attributed it to bulk effect.

Liu *et al.* [6] attributed this behavior to surface oxides/hydroxides impeding hydrogen entry, and the amount of surface coverage to be changing with cathodic charging time due to the reduction of surface oxide/hydroxide layer. They suggested applying a "pre-conditioning" treatment of the surface consisting in maintaining the entry face at a cathodic potential for a long time (48 h) to get rid of the oxides before performing the actual permeation test. Casanova and Crousier [10] also observed this double rise shape and tried to investigate two hypotheses that explain the causes of this shape: modification of the passive film on the detection side or the reduction of the oxide on the input side. Their results proved the former hypothesis wrong and they adopted the latter. Van den Eeckhout *et al.* [11] also assumed that these abnormalities in hydrogen permeation behavior was caused by surface reaction. They

* Corresponding author.
E-mail address: sarah.alzein@emse.fr (S. Alzein).

https://doi.org/10.1016/j.corsci.2024.111998
Received 27 November 2023; Received in revised form 6 March 2024; Accepted 17 March 2024
Available online 18 March 2024

tried to control various permeation conditions (electrolyte, oxygen content, the applied charging current density, *etc.*) to limit the surface reactions and achieve a typical permeation behavior reaching a conclusion that the surface roughness and possible contaminations from the electrolyte are of high importance for realizing a stable entrance surface state. Bockris *et al.* [14] also studied the effect of temperature and electrolyte on the hydrogen permeation and concluded that some electrolyte ions (I^-, CN^- and naphthalene) enhance permeation by lowering the metal/adsorbed hydrogen bond, while other ions (valeronitrile, naphtonitrile, and benzonitrile) undergo vertical adsorption hindering the discharge of hydrogen ions into the metal surface.

However, in all the aforementioned studies, the possible effect of volume defects on the shape of the permeation curve is not considered. Numerous studies [8,14–17] have nevertheless suggested that volume defects, such as porosities or microcracks, either pre-existing or formed under the influence of hydrogen, could affect the shape of the permeation curve. By absorbing a fraction of the hydrogen in gaseous form, these volume defects delay, or even prevent, the establishment of the steady-state diffusion regime. Dillard [17] and Raczinski *et al.* [15,18] have also observed that fusion zone iron is much less sensitive to this phenomenon than Armco iron, suggesting a possible role of pre-existing physical or chemical imperfections prior to hydrogen loading in Armco iron.

After all these extensive studies, researchers still have not reached an agreement on the causes of the abnormal permeation behavior or the mechanism behind each step. This encouraged this study where the causes behind this phenomenon will be experimentally investigated in an attempt to understand the underlying mechanisms and simulating them using a numerical model.

This paper aims to investigate whether the cause of abnormalities in hydrogen permeation is related to a surface reaction or a bulk reaction. Pure iron was used to avoid complexities in the microstructure that might interfere with the results. Different strategies to question the possible bulk or surface effects were adopted like using (or not using) Pd coatings, or varying the specimen thickness. The effect of hydrogen fugacity was studied as well. In addition, the possible effect of pre-existing bulk micro-porosity suggested in literature [7,15] was studied in detail. To achieve this, pure iron containing some amount of micro-porosity was prepared. It has been shown that micro-porosity may reversibly trap hydrogen at room temperature [7]. This may affect the permeation behavior and possibly explain the abnormal shape of the permeation curve. For better understanding, the permeation experiments were numerically replicated using the model proposed by Yaktiti *et al.* [19], that simulates hydrogen transport in a material containing micro-porosity, where hydrogen recombination can take place. In contrast to the more common "effective medium" models used for hydrogen diffusion and trapping in lattice defects, the Yaktiti model is particularly well suited for sparse traps (here micro-porosities) where a correct description of the hydrogen concentration field between traps is needed.

2. Materials and methods

2.1. Experimental methods

2.1.1. Material and sample preparation

The material used was pure iron (>99.998%wt-Fe), fabricated in the laboratory by melting under vacuum in a cold silver crucible. The impurity content was measured using Interstitial Gas Analysis. It was less than 20 wt ppm, with each of the C, N, O and S contents being less than 5 wt ppm. The material obtained in the as-solidified state usually has porosity defects with different sizes and shapes. There are two major reasons for the porosity formation during solidification: shrinkage and gas evolution [20,21]. Shrinkage porosity is generally localized at the last zones to solidify [20]. The shape of this type of porosity is usually not spherical and it takes the form of the remaining space between dendrites [22]. On the other hand, gas porosity is caused by the evolution of the dissolved gases during solidification. They have spherical or ellipsoidal shapes [22]. For our samples, the as-solidified material was hot-forged in the form of an iron rod of 20 mm diameter. The forging conditions were so that the micro-porosity inherited from the solidification process was not completely suppressed. A heat treatment, to eliminate defects and dislocations caused by forging, was performed in a sealed vacuum tube at 950°C for 1 hour, followed by slow cooling. This resulted in average grain size of 700 μm and hardness of 58±2 HV. For electrochemical permeation, different circular samples of thickness around 1 mm and 2 mm were then cut from the rod. Both sides of the samples were mechanically polished down until a 1 μm mirror finish.

2.1.2. Porosity fraction measurements

The presence of porosities was validated using SEM and hydrostatic weighing technique, using the same procedure as in [7]. Hydrostatic weighing technique allows the measurements of the real density of the sample. By comparing the density of a porous and non-porous sample, the porosity fraction can be obtained [7]. The typical specimen mass used for hydrostatic weighing was around 2.5 g.

Optical microscopy and image processing were also used to obtain more data on the porosity statistic. Based on basic topological rules, the surface porosity fraction obtained from image thresholding was used as a close estimation of the volume porosity fraction of the sample. Other characteristics as the average porosity diameter or the aspect ratio were determined as well. Finally, the inter-porosity distance, which is a 3D parameter, was extrapolated through the 2D data following Eq. (1):

$$d = r\left(\frac{4\pi}{3f}\right)^{1/3} \tag{1}$$

where r is the average porosity radius and f is the porosity fraction.

2.1.3. Electrochemical permeation

Electrochemical permeation tests were performed, employing the method developed by Devanathan and Stachurski [9,23]. The experimental setup is composed of two compartments. Each compartment was equipped with a saturated calomel reference electrode (SCE), a platinum auxiliary electrode and a common working electrode which was a circular-shape disc sample of the material under study. Each compartment was filled with a 0.1 M NaOH aqueous solution prepared using high resistivity (18 MΩ cm) deionized water. The solution was deaerated by nitrogen bubbling before and during the entire permeation test. All permeation tests were performed at room temperature (25°C ±1°C). In this technique, a thin sample is cathodically charged by potentiostatic or galvanostatic polarization at the entry side and hydrogen desorption is detected from the exit side. In the case of potentiostatic charging, the chemical activity of hydrogen at the specimen surface is fixed, so a constant subsurface hydrogen concentration C_0 can be maintained throughout the permeation test. In this study, we ran a few experiments under galvanostatic conditions (Fig. 8). However, the potentiostatic charging was used most. We adopted this approach because it is more rigorous from a thermodynamic point of view and since it is the approach used in the numerical part where a fixed hydrogen subsurface concentration is imposed. Going for galvanostatic charging would not guarantee a constant C_0 at the surface which is why it was abandoned.

Fig. 1 provides an illustration of the typical hydrogen permeation curve. The effective diffusion coefficient, D_{eff} (m^2/s) can be calculated using the time lag method from the permeation rise transient [24,25] as provided by Eq. (2).

$$D_{eff} = \frac{e^2}{6t_{lag}} \tag{2}$$

Where e is the sample thickness (m), and t_{lag} (s) represents the time when

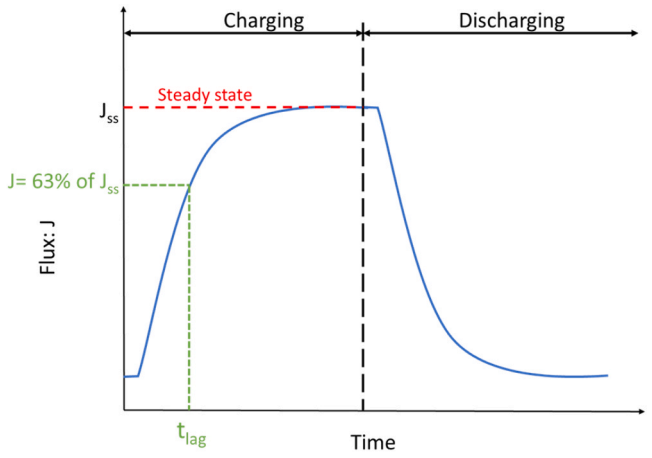

Fig. 1. Typical flux curve obtained during a permeation experiment showing the charging (rise) and discharging (decay) steps.

the current density at the exit side is equal to 0.63 of the steady-state current density.

2.2. Numerical model

The non-equilibrium model used in this work was previously published by Yaktiti *et al.* in [19]. It allows the local description of hydrogen diffusion and trapping into porosities. Unlike most diffusion-trapping models, this is not an effective environment model. It makes it possible to clearly describe the concentration field between the traps. It is based on a "non-equilibrium thermodynamics approach", where the flux of solute between two phases is governed by the difference in chemical potential. Based on that, an expression of hydrogen flux due to the hydrogen recombination/dissociation reaction at the bulk-cavity interface was developed. This model takes into consideration both the diffusion and the bulk-cavity interface reactions. The diffusion equation is solved using the Finite Element Method implemented in the Comsol software.

2.2.1. Geometry, initial and boundary conditions of the model

The simulations were conducted on a three-dimensional configuration, illustrated in Fig. 2(a), which shows one of the simulation domains

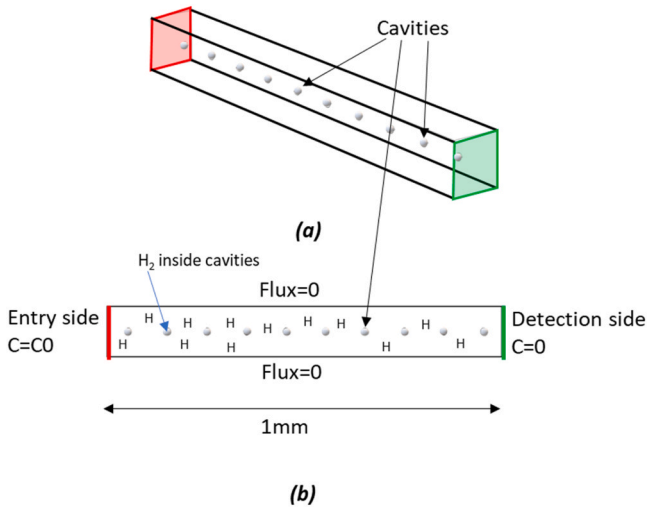

Fig. 2. (a) 3D representation of the model domain containing 10 cavities; (b) 2D representation of the model domain showing the initial and boundary conditions. For an easier representation of the numerical model, 10 cavities are represented but simulations were performed with 50 cavities.

utilized in this study. It represents an elementary representative volume of the permeation sample with spherical pores homogeneously distributed. A cross-sectional perspective of this setup is displayed in Fig. 2(b). In order to avoid numerical problems, non-zero initial conditions were imposed for the hydrogen concentration in the bulk (which was set at 0.001 mol/m^3), and for the pressure inside the cavity (which was set at ~0.1 MPa). These set values were checked to have no impact on the final results of the simulations. As for the boundary conditions, zero concentration was assumed on the right side of the box corresponding to the detection side of the permeation experiment. Conversely, the opposing side had a constant fugacity (corresponding to a constant concentration) imposed, representing the charging side of the permeation test. Additionally, periodic boundary conditions were applied along the lateral edges, where a hydrogen flux was maintained at zero. Due to these periodic boundaries, the fundamental simulated unit modeled here is representative to a 3D network of porosities.

A 3D simulation box is used for the calculations, with permeation length of 1 mm and a side equal to the inter-porosity distance representative of a single unit of the network of porosities in the sample. A box containing 50 cavities 1.4 μm in radius and an inter porosity distance of 0.2 mm was used, resulting in a volume porosity fraction of 0.14%. These input parameters were chosen similar to the porosity characteristics measured experimentally.

2.2.2. Recombination flux at the bulk-cavity interfaces

The numerical model lies on the introduction of a local recombination/dissociation flux at the bulk-cavity interface (Eq. 3) that allows hydrogen to recombine into H_2 inside the cavities [19,26,27], or H_2 to dissociate back to dissolved H into the bulk.

$$J_I = Q \times \left[C_I - K_H \times \sqrt{f} \right] \tag{3}$$

Where J_I is the hydrogen flux at the bulk-cavity interface, Q is a kinetic factor, C_I is the hydrogen concentration at the interface, K_H is the hydrogen solubility, and f is the hydrogen fugacity. The term in brackets is related to the difference in hydrogen chemical potential between the bulk and the cavity. When this term is positive (resp. negative), the hydrogen flux is directed towards the cavity (resp. the bulk), thus increasing (resp. decreasing) the cavity pressure. In a previous work [19], the kinetic factor Q was set as a constant ($Q = 10^{-4} m.s^{-1}$) high enough that the limiting step was not the recombination/dissociation reaction but rather the diffusion around the cavities. In the present work, the effect of various values of Q is studied, without any prior assumption of "diffusion-limited process" (high values of Q) or "recombination reaction-limited process" (low values of Q).

In this aspect, a modification of a significant importance was introduced to the model. This modification tackles the shortcomings of the previous model that considers hydrogen recombination and dissociation processes have the same rate which may not be the case in reality. The new modified model allows the kinetic factor Q is to have two different values depending on the sign of the term $\left[C_I - K_H \times \sqrt{f} \right]$. This allows us to study the effect of having different reaction rate for the recombination process ($2H_{abs} \rightarrow H_2$) and for the dissociation process ($H_2 \rightarrow 2H_{abs}$), as proposed in sub-section 4.4

3. Experimental results and discussion

3.1. Material characterization

Fig. 3 shows an optical image (a) and an SEM image (c) of a cross-section of the material prior to any permeation experiments. Pores are clearly identified by both optical (see black arrows) and electron microscopy. The iron used is very pure (> 99.998%wt), which considerably limits the risk of observing inclusions instead of pores. EDX analysis confirms the absence of any inclusion or oxide. Hence, the presence of

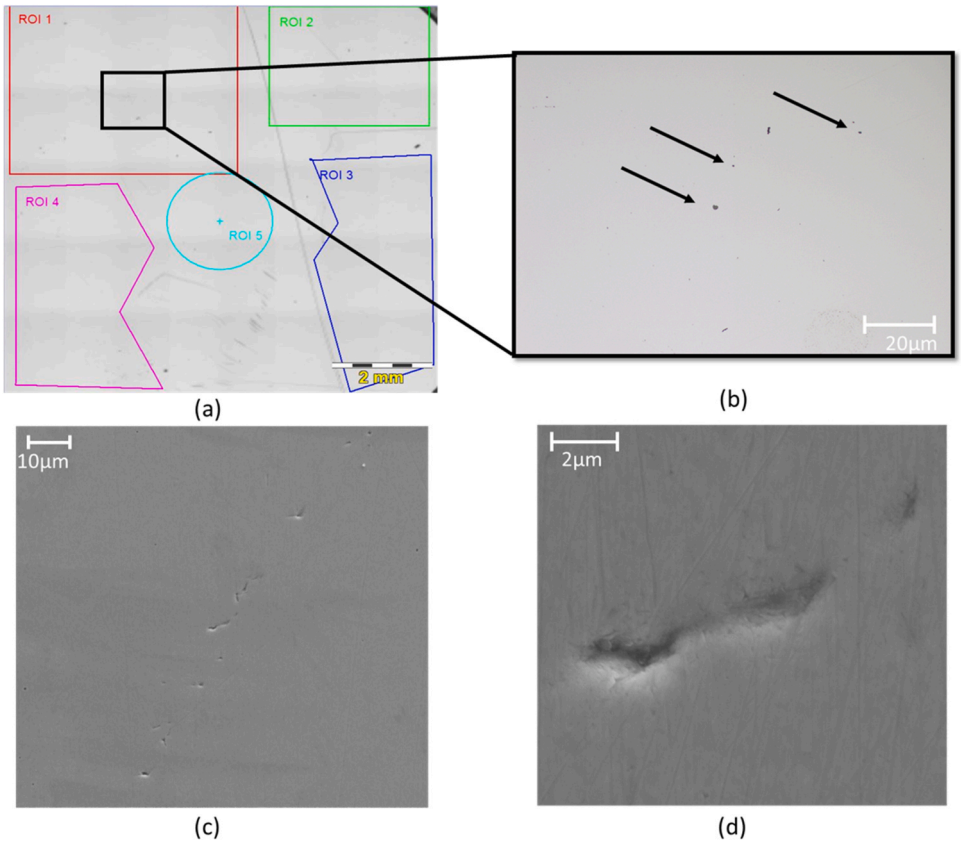

Fig. 3. (a) Optical imaging showing the entire sample divided to regions of interests. (b) Optical image showing pores contained in the sample prior to hydrogen permeation (the black arrows pointing at pores). (c) SEM image showing pores before permeation and (d) SEM image of a pore at high magnification.

porosities is confirmed by imaging and chemical analysis. Additionally, hydrostatic weighing technique confirms a porosity fraction between 0.1% and 0.2%, depending on the measured sample as presented in Table 1.

After confirming the presence of the porosities, optical microscopy was used to characterize the size and distribution of porosities. High resolution optical images were obtained on three different samples. The images were divided into several regions of interest that had no big defects (scratches, flutes) viewed in greyscale were only extremely dark elements are taken into consideration, as seen in Fig. 3(b). Several filters were used to eliminate remaining scratches and any extremely distorted and elongated (needle like) shapes. Statistics were performed on the filtered greyscale images to extract porosity data (Table 2). Note that more than 99% of the porosities have an average diameter between 1 µm and 5 µm.

3.2. Description of the abnormal curve

Hydrogen permeation tests were performed on the pure iron samples resulted in curves that has different shape from typical permeation curves. Those results were reproducible and repetitive over several samples under different charging conditions.

Fig. 4 shows the permeation rising and decaying transients that show clearly the abnormal shape. For the rising transient presented in Fig. 4 (a) and (c), this shape is characterized by a first short and fast rise that starts a few seconds after the beginning of charging until reaching a plateau after ~ 300 s. This plateau can only be considered as a pseudo-steady state since it only lasts till ~600–700 s where the curve starts its second rise. The second rise is slow and long and is followed by the final stable steady state that is attained after ~ 3×10^4 s from the beginning of charging.

For the decaying transient presented in Fig. 4(b) and (d), the shape is also very different from the typical shape. It is characterized by a fast decrease, followed by a non-zero pseudo-plateau, and then a very slow decay to zero flux. It is noticeable that the time needed to achieve final steady-state upon charging and the time needed to reach zero flux upon decaying are of the same order ([3,4]x10^4 s). This very long time needed to completely discharge the specimen was already observed by Raczinski [18] on Armco iron and by Yaktiti [7] on a low alloy steel, and was attributed to reversible trapping of hydrogen in volume defects.

The permeation curves shown in Fig. 4 were used to calculate the effective/apparent diffusion coefficient from the time lag equation (Eq. (1)). Results showed that for the first rise the effective diffusion coefficient is 2.1 $\times 10^{-9}$ m^2/s, which is in the range as the lattice diffusion coefficient of hydrogen in iron valued between 10^{-10} and 10^{-8} m^2/s

Table 1
Porosity fraction of 3 samples calculated using hydrostatic weighing technique.

Sample	Porosity Fraction
Sample 1	0.13%
Sample 2	0.14%
Sample 3	0.16%

Table 2
Porosity features measured using optical image processing.

Number of porosities studied for statistic	10298
Total surface area studied (mm^2)	49.15
Average diameter (µm)	2.2 ± 2.1
Aspect ratio	1.5 ± 0.8
Porosity fraction (%)	0.141
Inter-porosity distance (µm)	16.6

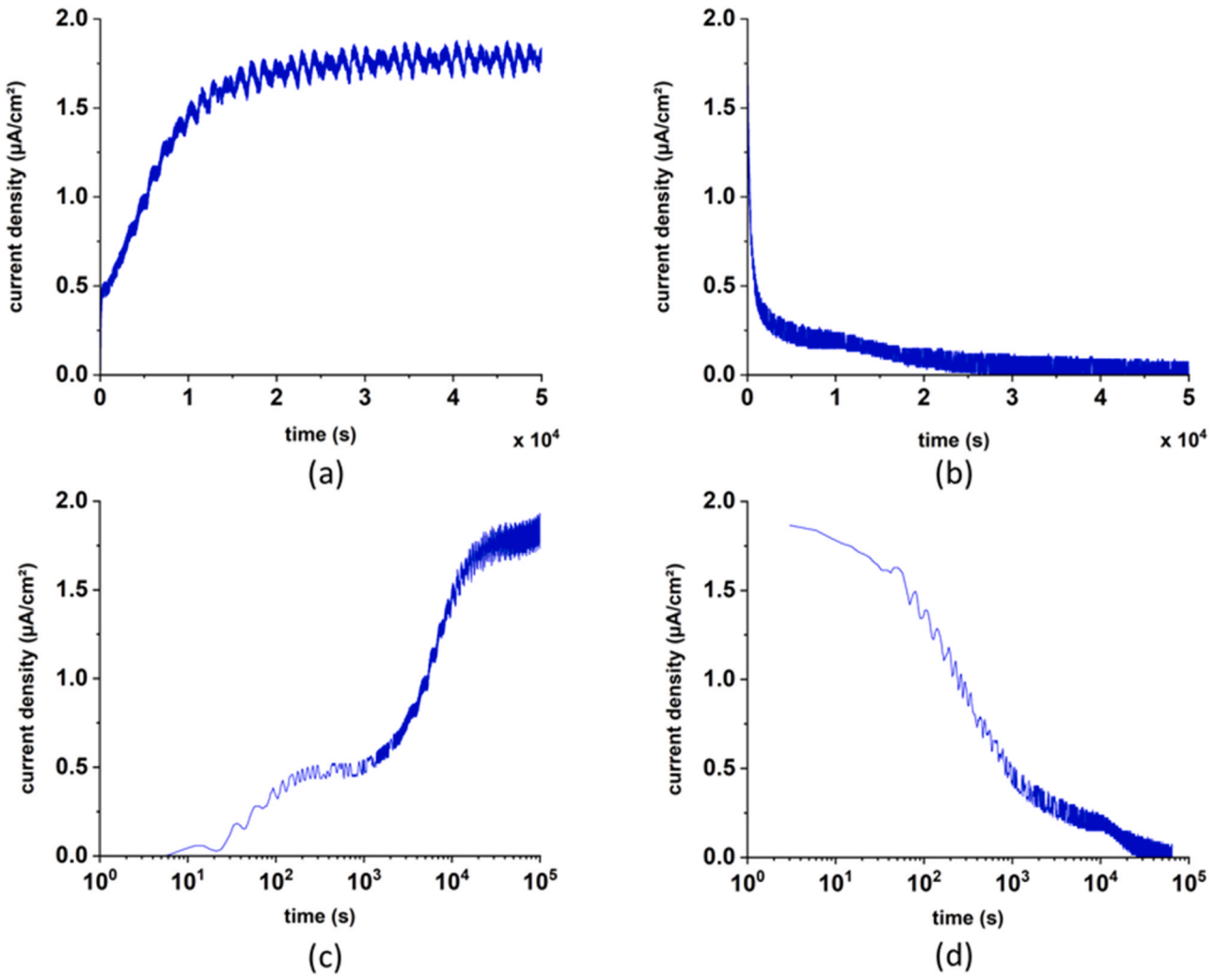

Fig. 4. Electrochemical hydrogen permeation results for a 1 mm sample charged at −1500 mV/SCE at 25°C in a 0.1 M NaOH aqueous solution. (a) and (c) rising transient; (b) and (d) decaying transient. (c) and (d) are in log timescale.

[28]. On the other hand, the second rise was much slower and the corresponding effective diffusion coefficient was 2.6 $\times 10^{-11}$ m^2/s.

From the diffusion data, it is clear that the first rise of the permeation curve corresponds to hydrogen diffusing through the bulk of the sample, whereas the second rise corresponds to a different phenomenon. This phenomenon is causing the 'double-rise' shape of the permeation rising transient and should be investigated further to understand its causes and how it is affected under different conditions.

3.3. Surface or bulk effect?

3.3.1. Effect of palladium coating

A sample was coated with a thin palladium layer by sputter Physical Vapor Deposition (PVD) on both sides after being polished. The thickness was controlled during the deposition process by adjusting the sputter current and the sputter time. The obtained thickness value was in the range 18–30 nm. The Pd-coating would act as a protective layer of the surface of the specimen used since it is much less reactive than iron. A permeation experiment was performed at −1650 mV/SCE. The results are presented in Fig. 5. The obtained permeation curve clearly shows the abnormality in the shape characterized by a double rise.

The low reactivity of Pd should protect the surface from any parasitic chemical reactions. However, the double rise shape is still observed. These results do not support the assumption provided by some researchers [6,10,11] that the 'double rise' permeation curve is due to surface reactions.

3.3.2. Effect of thickness

In order to confirm whether the cause behind the abnormal double rise shape is a surface or a bulk effect, it is proposed to conduct experiments on two different sample thickness (e=1 mm and e=2 mm). Electrochemical permeation tests were performed under same conditions on two samples that were prepared identically with the thickness as the only difference between them. The results are presented in Fig. 6. The results show that the rising permeation transients of both samples had the 'double rise' shape. However, the rises were slower for the thicker sample. After increasing the thickness by a factor of two, the time frame was shifted by a factor of 4. For example, the steady-state is reached at $\sim 10^4$ s for the 1 mm sample and at $\sim 4 \times 10^4$ s for the 2 mm sample. These results are an indication of a bulk volume effect taking place rather than a surface effect. Since the two sample surfaces were identically prepared, the rise corresponding to any parasitic surface reaction, if true, should not have underwent the delay by a specific factor as observed.

The effect of thickness combined with the effect of Pd-coating seem to refute the theory that the abnormal 'double rise' shape is a surface effect. The simplicity of the material used (pure iron) that has no complexities in the microstructure except for the micro porosities leads us to pose a hypothesis that this abnormal shape is caused by the porosities present. The first rise is caused by hydrogen diffusing through the iron

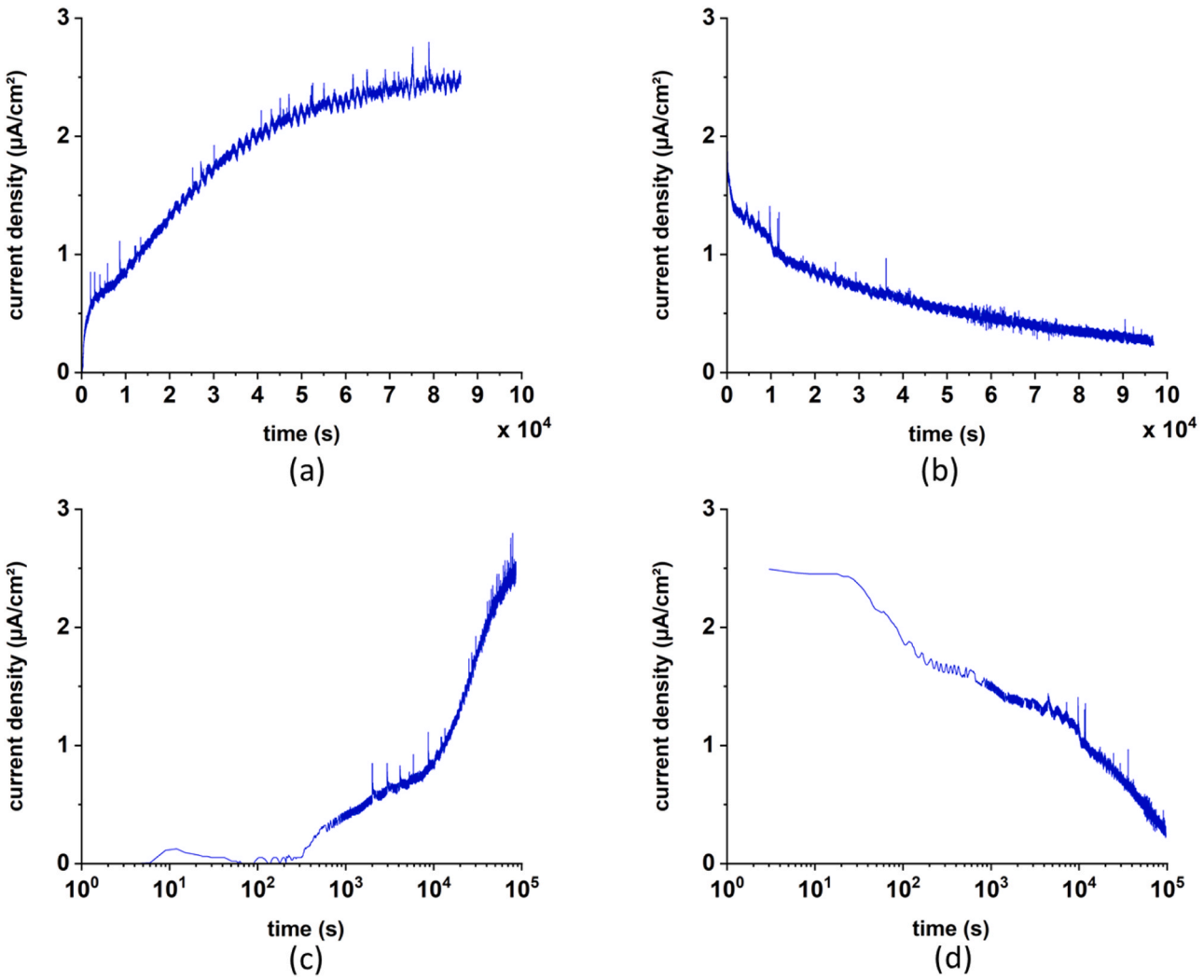

Fig. 5. Electrochemical hydrogen permeation results for a palladium coated sample on entry and exit sides of 1.21 mm thickness charged at −1650 mV/SCE. (a) rising transient and (b) decaying transient. (c) and (d) are in log timescale.

lattice. The first plateau corresponds to a pseudo-steady state, characterized by two fluxes of hydrogen: one flux escaping the specimen (the one measured in the permeation experiment) and another one "leaking" into the porosities. Once the pores start to fill, more hydrogen is available to diffuse causing the second rise. The actual steady state (second plateau) is only obtained when the hydrogen pressure in each porosity is equilibrated with the local lattice hydrogen concentration.

3.4. Effect of fugacity

To further understand the double rise behavior and to validate the proposed assumption, the hydrogen charging fugacity was varied. The results presented in Fig. 7 showed that after charging for significant time periods, only a single rise was observed at low hydrogen concentration (low cathodicity) and the double rise shape becomes more prominent at higher hydrogen concentrations (high cathodicity). At low hydrogen concentration (low fugacity), low amounts of hydrogen are introduced into the sample causing a lower first plateau and less hydrogen to be available to enter the pores. This means that the amounts of hydrogen permeating the sample are too low to fill the pores fast enough causing us to only see the first rise. In this case, in order to obtain the 'double rise' shape, the sample should be charged for very long periods of time.

3.5. Damage inflicted on material after hydrogen charging

Beck *et al.* [8] results showed that repeated hydrogen charging causes a decrease in the hydrogen permeability of the material, but these results occurred after charging at severe conditions (> -5 mA/cm^2). The authors attributed the decrease in permeability after repeated charging to irreversible damage in the material due to hydrogen. To investigate further, two permeation tests were performed under the same conditions on the same sample. The sample was galvanostatically charged at -3 mA/cm^2 then completely discharged, followed immediately by a second run under the exact same conditions. The obtained results showed a significant decrease in the steady state current density between the first and second runs as presented in Fig. 8. In addition, for the two experiments, the steady state current is decreasing over time (which was already observed in Fig. 6 and Fig. 7). These two observations suggest that damage is indeed occurring in the specimen during permeation.

SEM images obtained of samples after hydrogen permeation at −1650 mV/SCE can be seen in Fig. 9. The charging face of the sample exhibits blisters (Fig. 9(a)), which look like round bubbles at first glance, as well as some cracks (Fig. 9(b)). In cross-section (Fig. 9(c) and (d)), cracks and pores are visible as well. It should be noted that pores shown in Fig. 9(d) do not correspond to those initially present in the material: they are much more numerous and concentrated in particular areas on

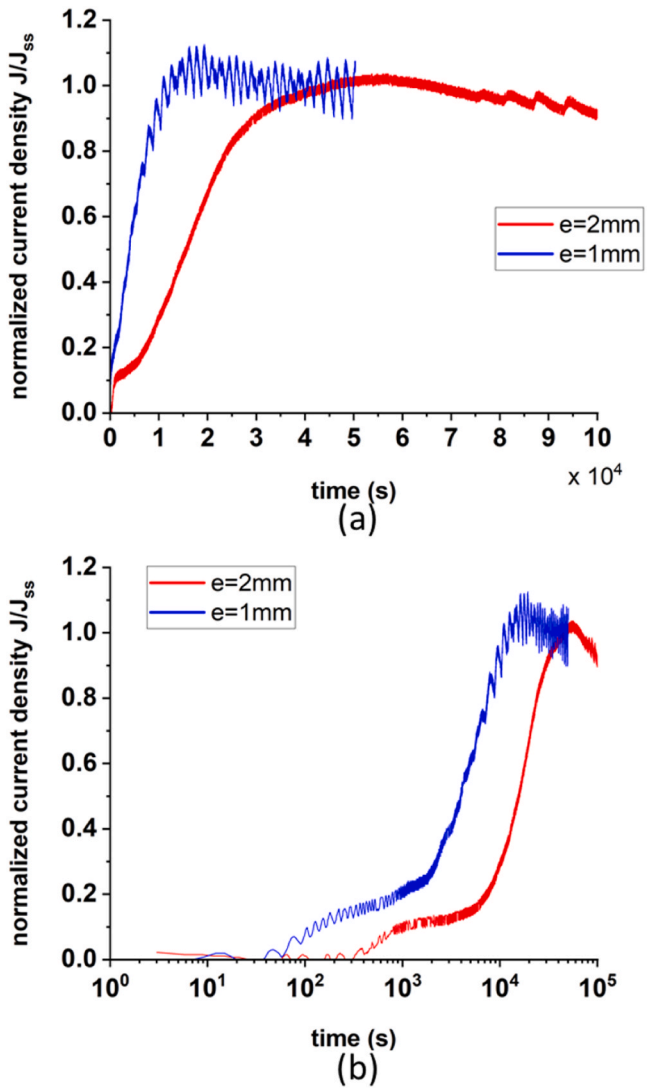

Fig. 6. Electrochemical hydrogen permeation results for two samples having different thicknesses, e= 1 mm and e= 2 mm charged at −1650 mV/SCE. Normalized current density in (a) linear timescale and (b) log timescale.

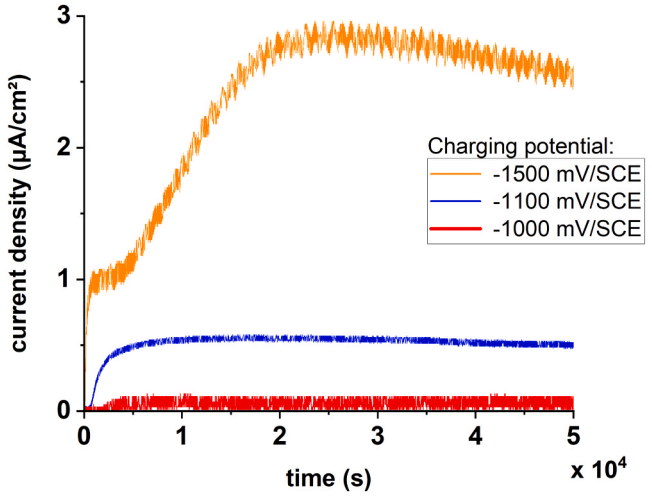

Fig. 7. Electrochemical hydrogen permeation results for three samples identically prepared having a 1 mm thickness. Permeation charging current was varied between −1500 mV/SCE to −1000 mV/SCE.

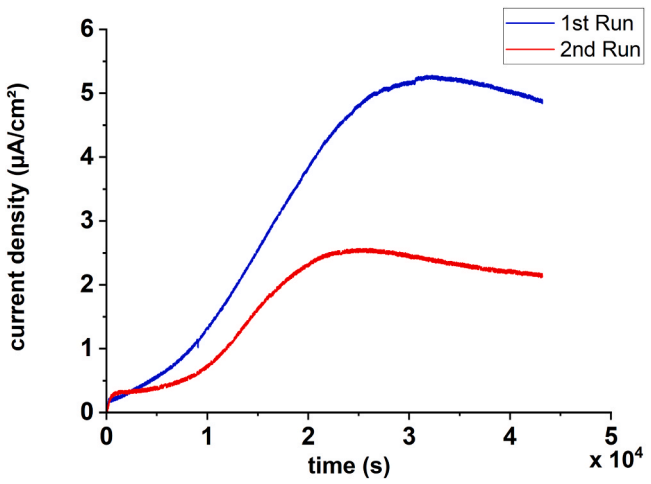

Fig. 8. Electrochemical hydrogen permeation rising transients for the same sample charged at −3 mA/cm^2, then discharged, then charged again under same conditions.

the specimen. This damage caused by hydrogen charging is similar to that observed by Tiegel *et al.* [16].

These results help highlight the severity of the effect hydrogen charging has on a sample and the effect it may inflict on the permeation results of samples that were charged previously even if those samples were left to discharge completely. In the second permeation run shown in Fig. 8, the increased defective volume due to additional cracks and pores results in a longer pseudo-steady state plateau (first plateau) compared to the first run. The decreasing steady-state current can also be explained by a continuously increasing defective volume. This corresponds to a situation already depicted in literature, where the increasing defective volume can make the establishment of the actual steady state permeation difficult [8,18].

Analyzing the damage inflicted after hydrogen charging, especially the severe blistering occurring leads us to question if the 'double rise' shape of the permeation curves is influenced by the formation of blisters. To clarify this, an interrupted permeation test was conducted where charging was stopped before the onset of the second rise. Fig. 10 shows the interrupted rising transient, together with the complete transient obtained on another specimen in the same conditions (the blue permeation curve of Fig. 6). In the two cases, the double-rise behavior is clearly observed. SEM inspection of the specimen surfaces showed blistering for the specimen that underwent the complete rising transient (Fig. 9(a)), whereas no blister could be found on the other specimen. This suggests that blistering occurs relatively late in the permeation process and is not the root cause of the double-rise behavior. This is consistent with the observations of Yaktiti *et al.* [7] where the same double-rise behavior was obtained on a low alloy steel containing micro-porosity, whereas no blistering was reported in that study.

4. Numerical results and discussion

4.1. Input parameters

In this part, the Yaktiti model [19] is used to simulate the hydrogen permeation across a specimen containing micro-porosity in order to check whether the presence of porosity can explain the double rise behavior. The input parameters of the model are listed in Table 2. Hydrogen solubility for pure iron was taken from [29]. The hydrogen diffusion coefficient used was calculated as an average of several apparent diffusion coefficients extracted from the first rise of several experimental curves using the time lag method. The porosity characteristics were obtained from experimental observations. The steady state hydrogen flux values J_{SS}^{exp} obtained for the charging potential of

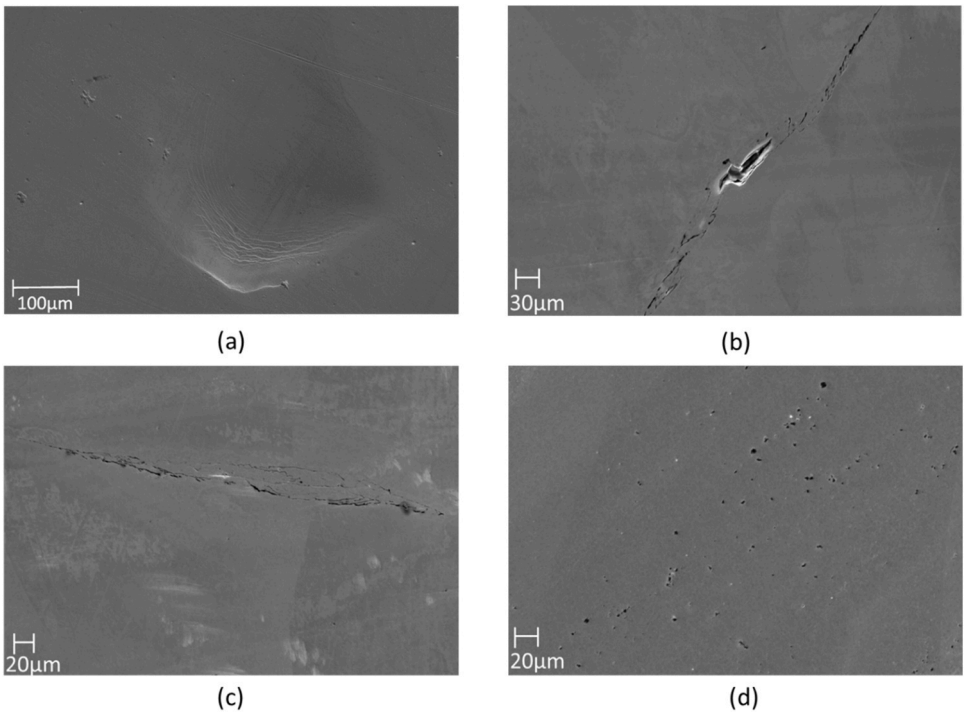

Fig. 9. SEM images showing the damage introduced to a specimen after permeation at −1650 mV/SCE. (a) and (b) are observations of the charging face showing a blister (a) and a crack (b). (c) and (d) are cross section observations of the specimen bulk showing a crack (c) and numerous pores concentrated in particular area (d).

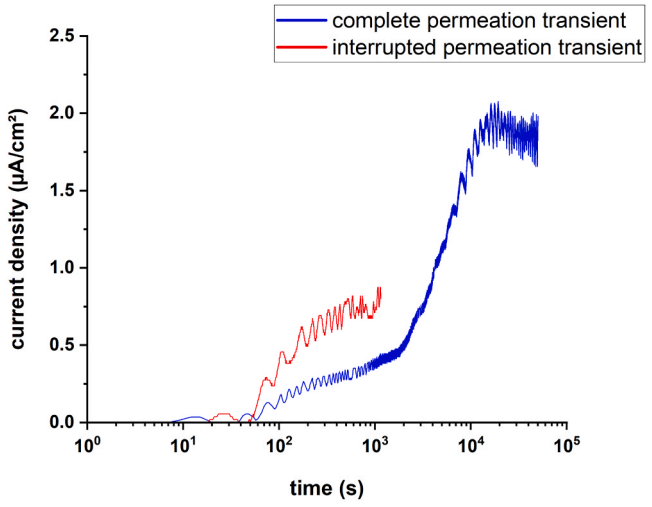

Fig. 10. Electrochemical hydrogen permeation results for two samples: one completely permeated and the other interrupted at the beginning of the second rise, charged at −1650 mV/SCE. The specimen thickness is 1 mm in both cases. Surface blistering is observed after the complete transient, but not after the interrupted one.

−1500 mV/SCE ($J_{SS}^{exp} = 1.8\mu A/cm^2 = 1.865 \times 10^{-7} mol\ H/m^2/s$, Fig. 4) was used to calculate the corresponding subsurface hydrogen concentration C_0 using Fick's law (Eq. (4)).

$$J_{SS}^{exp} = \frac{D \times C_0}{e} \rightarrow C_0 = \frac{e \times J_{SS}^{exp}}{D} = 1.884 mol \Big/ m^3 \quad (4)$$

where D is the lattice hydrogen diffusion coefficient and e is the permeation specimen thickness. Other C_0 values in the range [0.2512–2.512] mol/m^3 were also used as well in different simulations.

Table 3
Input parameters used in the numerical simulations.

Parameter	Values
Solubility K_H (mol/(m^3.bar$^{0.5}$))	0.003936 [29]
Diffusion coefficient D (m^2/s)	8.5 ×10^{-10}
Permeation length e (mm)	1
Temperature T (°C)	20
Porosity volume fraction X_p (%)	0.14
Kinetic factor Q (m/s)	[10^{-9}-10^{-3}]
Subsurface hydrogen concentration C_0 (mol/m^3)	[0.2512–2.512]
Number of porosities	50
Pore radius (µm)	1.4
Inter-porosity distance (µm)	20

4.2. *Effect of kinetic factor Q*

The kinetic factor Q affects the hydrogen flux at the bulk-cavity interface as presented in Eq. (2). It is used to quantify the kinetics of the hydrogen recombination or dissociation at the bulk-cavity interfaces [19]. The aim of the first simulations was to understand the effect of the kinetic factor. Fig. 11 shows the effect of Q on the permeation flux, Fig. 11 (a) and (b), and on the pressure inside the first cavity (cavity closest to charging side), Fig. 11 (c) and (d). For very low values of Q ($Q = 10^{-9}$ m/s), the permeation curves are the same as in the 0-cavity case where the rise begins at approximatively 50 s. For very high values of Q ($Q = 10^{-3}$ m/s), the permeation curves have the same shape as the case without porosities but is much slower where rise starts after around 2000 s. For intermediate Q values, the permeation flux exhibits a double rise shape where the first rise begins after around 50 s and the second rise begins as the cavity pressure significantly increases until the flux reaches its steady state values after the cavity pressure stabilizes.

Considering the rising transients (Fig. 11 (a) and (c)):

- For low kinetic rate ($Q = 10^{-9}$ m/s), the hydrogen recombination reaction at the cavity interface is extremely slow. This causes almost all of the hydrogen to diffuse through the bulk without filling the

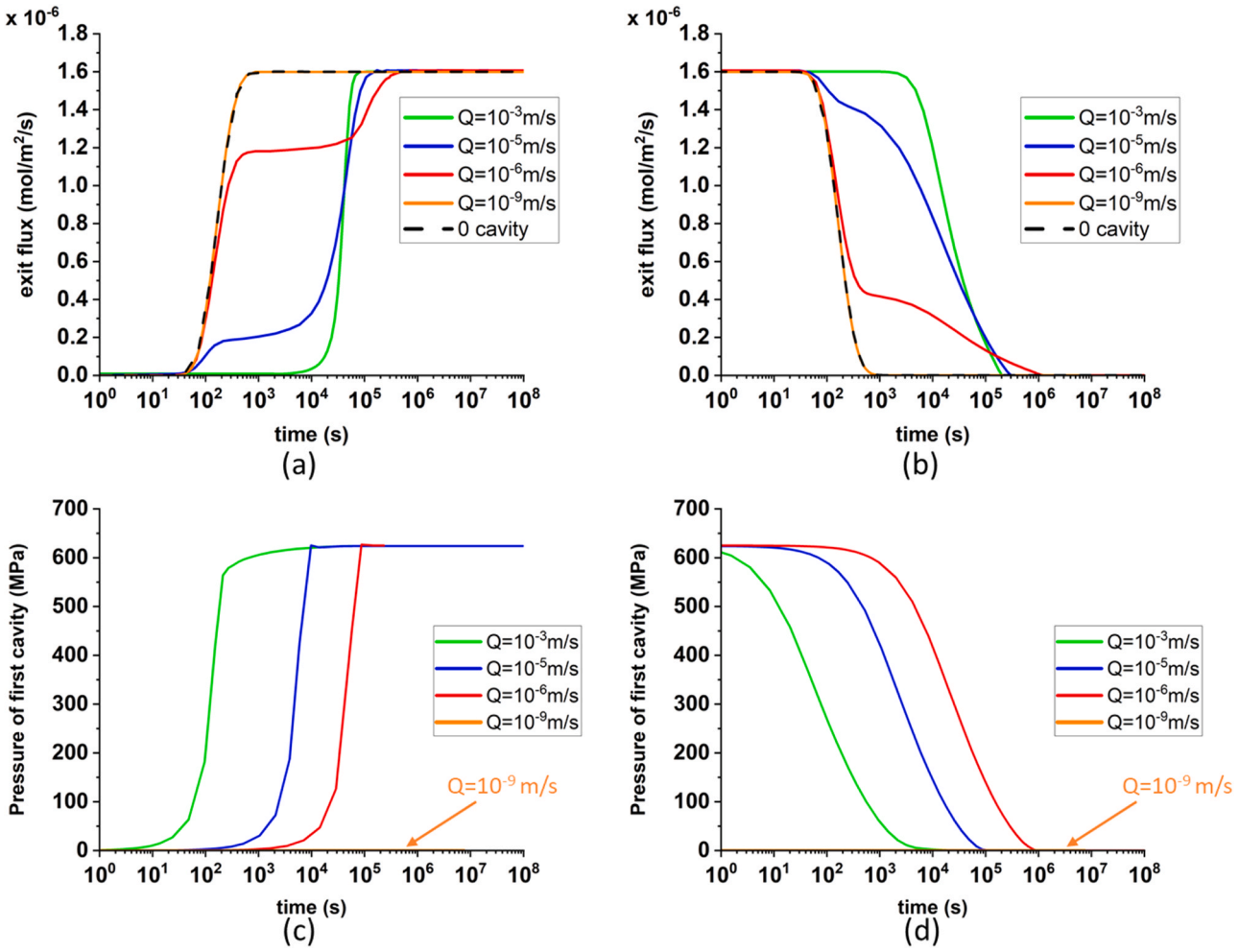

Fig. 11. Effect of kinetic factor Q on hydrogen permeation flux during (a) charging and (b) discharging; and on the pressure of the first cavity during (c) charging, and (d) discharging. ($C_0 = 1.884$ mol/m^3).

cavities which is why there is no accumulation of the pressure in the cavities in this case. Since very little (almost none) hydrogen is allowed into the cavities the hydrogen permeates as if there are no cavities present in the sample which is the reason behind the permeation flux of this case being equal to that of the 0-cavity case.

- For high kinetic rate ($Q = 10^{-3}$ m/s), the hydrogen recombination reaction at the cavity interface is extremely rapid. This means most of the hydrogen atoms entering the sample are being sucked into the pores allowing very little (almost none) hydrogen to permeate through the bulk until the cavities are filled to equilibrium. As shown in [19], this case corresponds to the local equilibrium situation, where the cavity pressure is in equilibrium with the surrounding hydrogen concentration at any time.
- For intermediate kinetic rates ($Q = 10^{-6}$ m/s and $Q = 10^{-5}$ m/s), the 'double rise' shaped curve is obtained. The first rise begins at the same time as the 0-cavity case proving that the first rise is due to hydrogen permeating through the iron lattice. The height and length of the first plateau depend on the kinetics of the cavity interface reaction, the faster the kinetics the shorter and lower the first plateau. Then, as more hydrogen is introduced into the cavities, more hydrogen permeates through the material causing the second rise that ends in the final steady- state plateau once all the cavities are filled to equilibrium.

Considering the decaying transients (Fig. 11 (b) and (d)):

- For low kinetic rate ($Q = 10^{-9}$ m/s), almost no hydrogen is present in the porosities, only hydrogen in the iron bulk lattice diffuses causing the observed fast drop which is similar to the 0-cavity case.
- For high kinetic rate ($Q = 10^{-3}$ m/s), hydrogen buildup in the cavities supplies hydrogen to the bulk sustaining a longer permeation flux at the steady state value. Again, this situation corresponds to the local equilibrium assumption.
- For intermediate kinetic rates ($Q = 10^{-6}$ m/s and $Q = 10^{-5}$ m/s), the stored hydrogen does not exit the cavities fast enough to sustain the steady state, so a sharp drop in hydrogen flux initially appears due to bulk hydrogen exiting the sample. Then, as the cavities start to significantly release some hydrogen (see the pressure drop in Fig. 11 (d)), a pseudo-plateau is observed in the permeation flux. The symmetry between the rising and decaying transients of Fig. 11 (a) and (b) is noticeable. For intermediate Q values, a pseudo-plateau is present on both *rising* and *decaying* transients, corresponding respectively to hydrogen being *trapped in* and *detrapped from* the cavities.

4.3. *Effect of fugacity*

The experimental results of Fig. 7 showed that the hydrogen charging fugacity affected the possible occurrence of the double rise behavior. At low fugacities, the 'double rise' could not be observed, possibly, due to the long time needed to fill the cavities. To further understand the effect of fugacity and to confirm the proposed theory, several simulations were

performed where the surface hydrogen concentration was varied to simulate the different charging conditions. Regarding the kinetic rate, an intermediate rate of $Q = 10^{-5}$ m/s was used to ensure the occurrence of a 'double rise' increasing transient. The results presented in Fig. 12 show that the second rise was slower at lower concentrations. To elaborate, lower hydrogen concentrations require more time to fill the cavities to equilibrium which is why the second rise is slower.

Observing Fig. 12 (c), and comparing it to some of the experimental values from Fig. 7 presented in Fig. 12 (d), it can be seen that after ~ 5 $\times 10^4$ s, the double rise is clear and the steady state is achieved for the high fugacity (high concentration) case. At the same time, the 'double rise' shape is not observed and the second rise has barely started in the low fugacity case. The double rise and the steady state will only appear much later at ~ [3,4] x 10^5 s. These results explain what was observed in the experimental curves in Fig. 12 (c) where only a single rise is observed at low fugacity in the time frame of the experiment.

4.4. Non-constant kinetic factor

The simulations presented in Fig. 11 show a certain symmetry between the rising and decaying transients: when an intermediate pseudo-plateau occurs *early* upon rising (i.e. at a relatively low flux value), a corresponding *early* pseudo-plateau (i.e. at relatively high flux value) is observed upon decaying (blue curves in Fig. 11 (a) and (b)). Similarly, if the pseudo-plateau occurs *later* upon rising, it also occurs *later* upon decaying (red curves in Fig. 11 (a) and (b)). On the other hand, the same symmetry is not observed in experimental results of Fig. 4, where the pseudo plateau occurs relatively early upon rising, but significantly later upon decaying. This suggests that the trapping and detrapping processes may have different kinetics.

At the bulk-cavity interface, two reactions take place: the recombination of atomic hydrogen into molecular hydrogen, and the dissociation of molecular hydrogen into atomic hydrogen. Although these reactions are the reverse of each other, they can have different kinetics. This can be modelled by setting a given value of Q for the recombination reaction, which is dominant during charging, and a different value for the dissociation reaction, which is dominant during the discharging. In practice, this is simply obtained by assigning different values of Q depending on the direction of the flux, inward or outward, as explained in the Materials and methods Section 2.2.2. Fig. 13 (a) and (c) show the simulations obtained for different Q values for flux entering and leaving the cavities. Comparing these results to the experimental results of Fig. 4 (c) and (d) shown again in Fig. 13 (b) and (d), they show very similar shapes: the pseudo-plateau upon rising occurs relatively early, whereas that upon decaying occurs much later. This would suggest that the kinetics of hydrogen detrapping from the porosity is indeed significantly slower that the trapping kinetics.

5. Conclusion

In this work, the causes of the abnormal 'double rise' shape of the hydrogen permeation rising transient has been studied by means of

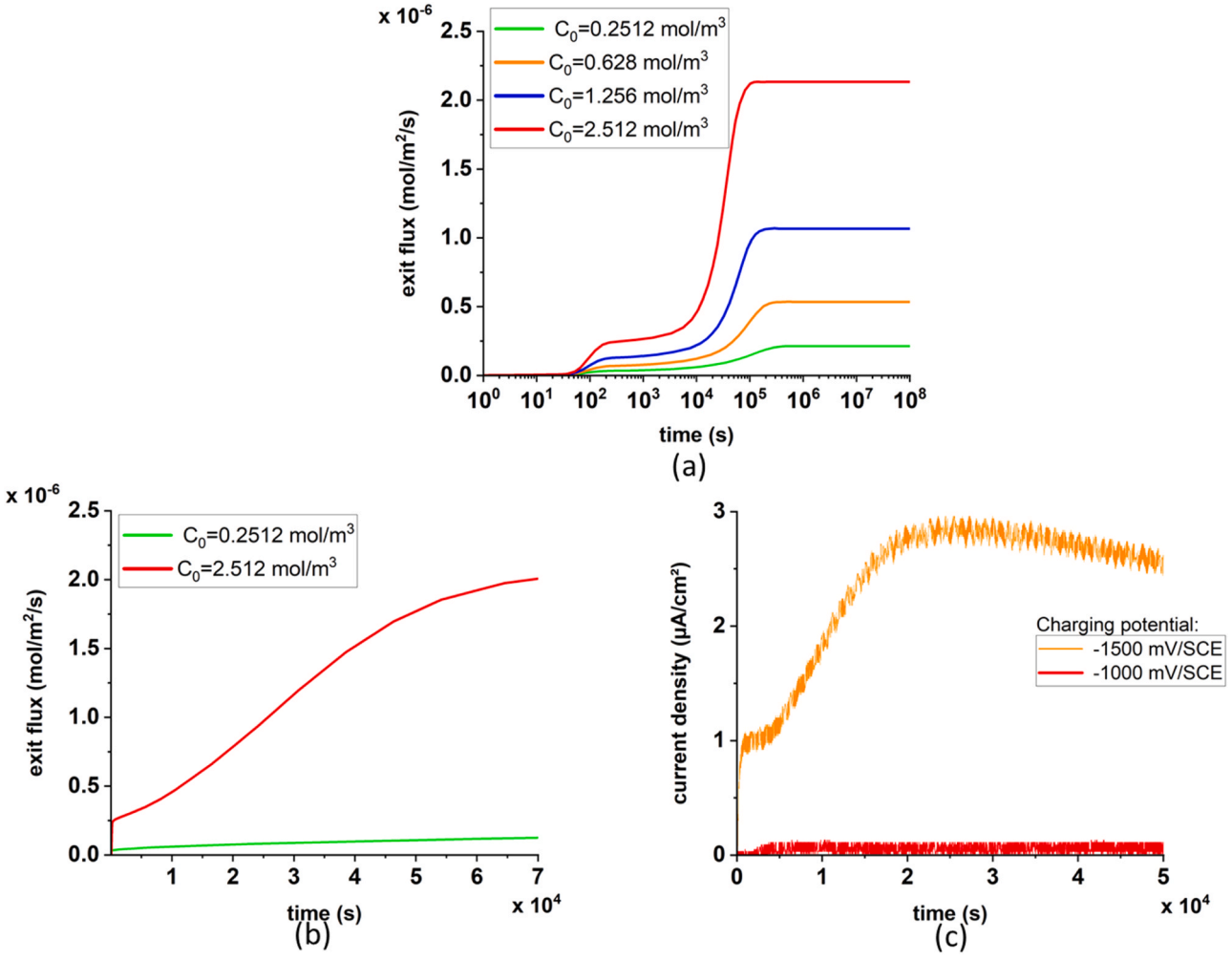

Fig. 12. Effect of subsurface hydrogen concentration C_0 (hydrogen fugacity). Simulated rising transients ($Q = 10^{-5}$ m/s) plotted with log time scale (a) and linear time scale (b). Experimental rising transients of Fig. 7 are shown in (c) for comparison.

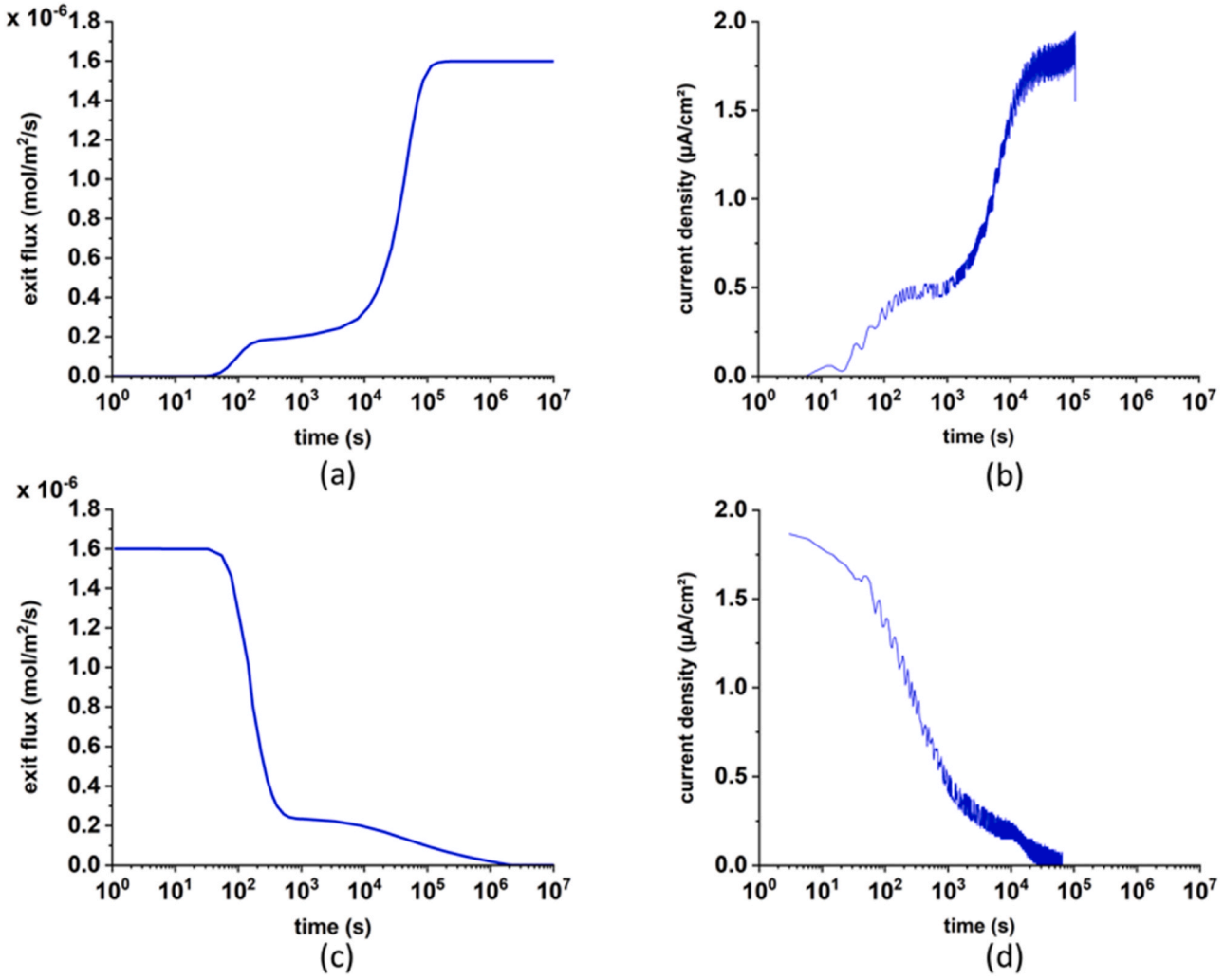

Fig. 13. Modelling of asymmetric rise (a), and decay (c) transients ($Q_{entering\ cavity} = 10^{-5}$ m/s; $Q_{leaving\ cavity} = 5 \times 10^{-6}$ m/s. $C_0 = 1.884$ mol/m^3. Experimental transients of Fig. 4 are shown in (b) and (d) for comparison.

electrochemical permeation conducted on pure iron containing micro-porosity. Also, the non-equilibrium numerical model previously developed by Yaktiti *et al.* [19] has been used to simulate hydrogen diffusion through the material, taking into account the trapping of gaseous hydrogen inside cavities.

In summary, the most significant findings of this study are:

- Electrochemical permeation tests performed as well as literature investigations prove that the 'double rise' shape is reproducible and is seen in pure iron as well as low alloy steels. The first rise is fast and corresponds to hydrogen lattice diffusion across the specimen. It is followed by a short pseudo-plateau, and a slow second rise until final steady state. Similar observations can be made on the decaying transients (although the rising and decaying transients are not perfectly symmetric): a fast decrease of the flux is first observed, followed by a non-zero pseudo-plateau, and then a very slow decay to zero flux. The time needed to achieve complete discharging is of the same order as that needed to obtain the permeation steady state upon charging, i.e. several days. This suggests that micro-porosity acts as reversible traps at room temperature, as already mentioned in literature.
- Electrochemical permeation tests performed on Pd-coated samples as well as samples with different thicknesses indicate that the 'double rise' shape is caused by a bulk effect rather than by parasitic surface reactions.
- The double rise behavior is not visible at low hydrogen fugacity, most presumably because the second rise only occurs at extremely long times.
- Inspecting the material after permeation using SEM showed significant damage inflicted on the surface and in the bulk of the material in form of blisters, cracks and additional porosity, even in the relatively "soft" H-charging conditions used in this study (no recombination poison used). This damage can cause unstable "steady state" permeation currents and significantly affect the shape of the second run rising transients.
- The Yaktiti model [19] was able to reproduce the double rise permeation behavior in the presence of micro-porosity, assuming limited recombination/dissociation reaction kinetics at the bulk-cavity interfaces. The permeation behavior upon decaying was also correctly captured by the model. The intermediate pseudo-plateaus observed on the rising and decaying transients are due to hydrogen trapping and de-trapping respectively in the micro-porosity.
- Numerical simulations showed that the asymmetry between the rising and decaying transients can be caused by the difference of kinetic rates between the recombination and dissociation reactions (hydrogen entering vs hydrogen leaving the cavities).
- Finally, after combining the results obtained from the permeation tests and numerical simulations, it is concluded that the abnormal

'double-rise' shape of the permeation curve is caused by the micro-porosities present in the material.

CRediT authorship contribution statement

Sarah Alzein: Writing – original draft, Methodology, Investigation, Formal analysis, Data curation, Conceptualization. **Frederic Christien:** Writing – review & editing, Visualization, Validation, Supervision, Project administration, Formal analysis, Conceptualization. **Alixe Dreano:** Writing – review & editing, Validation, Supervision, Conceptualization.

Declaration of Competing Interest

The authors declare that they have no known competing financial interests or personal relationships that could have appeared to influence the work reported in this paper.

Data Availability

Data will be made available on request.

References

[1] L. Zhang, M. Wen, M. Imade, S. Fukuyama, K. Yokogawa, Effect of nickel equivalent on hydrogen gas embrittlement of austenitic stainless steels based on type 316 at low temperatures, Acta Mater. 56 (2008) 3414–3421, https://doi.org/10.1016/j.actamat.2008.03.022.

[2] S.P. Lynch, Hydrogen embrittlement (HE) phenomena and mechanisms. in: Stress Corros. Crack., Elsevier, 2011, pp. 90–130, https://doi.org/10.1533/9780857093769.1.90.

[3] T. Hickel, R. Nazarov, E.J. McEniry, G. Leyson, B. Grabowski, J. Neugebauer, Ab initio based understanding of the segregation and diffusion mechanisms of hydrogen in steels, JOM 66 (2014) 1399–1405, https://doi.org/10.1007/s11837-014-1055-3.

[4] H. Zhao, P. Chakraborty, D. Ponge, T. Hickel, B. Sun, C.-H. Wu, B. Gault, D. Raabe, Hydrogen trapping and embrittlement in high-strength Al alloys, Nature 602 (2022) 437–441, https://doi.org/10.1038/s41586-021-04343-z.

[5] T. Timmerscheidt, P. Dey, D. Bogdanovski, J. Von Appen, T. Hickel, J. Neugebauer, R. Dronskowski, The role of κ-carbides as hydrogen traps in high-Mn steels, Metals 7 (2017) 264, https://doi.org/10.3390/met7070264.

[6] Q. Liu, A.D. Atrens, Z. Shi, K. Verbeken, A. Atrens, Determination of the hydrogen fugacity during electrolytic charging of steel, Corros. Sci. 87 (2014) 239–258, https://doi.org/10.1016/j.corsci.2014.06.033.

[7] A. Yaktiti, A. Dreano, J.F. Carton, F. Christien, Hydrogen diffusion and trapping in a steel containing porosities, Corros. Sci. 199 (2022) 110208, https://doi.org/10.1016/j.corsci.2022.110208.

[8] W. Beck, J.O. Bockris, J. McBreen, L. Nanis, Hydrogen permeation in metals as a function of stress, temperature and dissolved hydrogen concentration, Proc. R. Soc. Lond. Ser. Math. Phys. Sci. 290 (1966) 220–235, https://doi.org/10.1098/rspa.1966.0046.

[9] M.J. Danielson, Use of the Devanathan–Stachurski cell to measure hydrogen permeation in aluminum alloys, Corros. Sci. 44 (2002) 829–840, https://doi.org/10.1016/S0010-938X(01)00103-2.

[10] T. Casanova, J. Crousier, The influence of an oxide layer on hydrogen permeation through steel, Corros. Sci. 38 (1996) 1535–1544, https://doi.org/10.1016/0010-938X(96)00045-5.

[11] E. Van Den Eeckhout, K. Verbeken, T. Depover, Methodology of the electrochemical hydrogen permeation test: a parametric evaluation, Int. J. Hydrog. Energy 48 (2023) 30585–30607, https://doi.org/10.1016/j.ijhydene.2023.04.211.

[12] G. Fumagalli, F. Bolzoni, E. Fallahmohammadi, G. Re, L. Lazzari, Electrochemical methods for determining diffusion coefficient of hydrogen in steels, Corros. Eng. Sci. Technol. 50 (2015) 203–210, https://doi.org/10.1179/1743278215Y.0000000017.

[13] F. Bolzoni, E. Fallahmohammadi, G. Re, G. Fumagalli, M. Ormellese, L. Lazzari, Electrochemical Investigation of Hydrogen Diffusion in Pipeline Steels, in: NACE - Int. Corros. Conf. Ser., NACE International, Milano, Italy, 2013. https://www.researchgate.net/publication/236325687.

[14] J.O. Bockris, J. McBreen, L. Nanis, The hydrogen evolution kinetics and hydrogen entry into a-iron, J. Electrochem. Soc. 112 (1965) 1025, https://doi.org/10.1149/1.2423335.

[15] W. Raczynski, S. Talbot-Besnard, Coefficient de diffusion de l'hydrogène cathodique dans le fer de zone fondue et le fer Armco, Comptes Rendus Hebd, Séances Acad. émie Sci. Ser. C. t269 (1969) 1253–1256.

[16] M.C. Tiegel, M.L. Martin, A.K. Lehmberg, M. Deutges, C. Borchers, R. Kirchheim, Crack and blister initiation and growth in purified iron due to hydrogen loading, Acta Mater. 115 (2016) 24–34, https://doi.org/10.1016/j.actamat.2016.05.034.

[17] J.L. Dillard, Etude de la Diffusion, de L'hydrogene Cathodique dans le fer par detection electrochimique, M. éM. Études Sci. Rev. M. éTall LXVII (1970) 767–775.

[18] W. Raczynski, S. Talbot-Besnard, Perméabilité de l'hydrogène cathodique à travers des membranes de fer de zone fondue et de fer industriel, Comptes Rendus Hebd, Séances Acad. émie Sci. Ser. C. t269 (1969) 294–297.

[19] A. Yaktiti, A. Dreano, R. Gass, T. Yvert, J.F. Carton, F. Christien, Modelling of hydrogen diffusion in a steel containing micro-porosity. Application to the permeation experiment, Int. J. Hydrog. Energy 48 (2023) 14079–14094, https://doi.org/10.1016/j.ijhydene.2022.12.208.

[20] R.D. Pehlke, Formation of porosity during solidification of cast metals, in: S. Katz, C.F. Landefeld (Eds.), Foundry Process, Springer US, Boston, MA, 1988, pp. 427–445, https://doi.org/10.1007/978-1-4613-1013-6_17.

[21] N. Mahomed, Shrinkage porosity in steel sand castings: formation, classification and inspection, in: Z. Abdallah, N. Aldoumani (Eds.), Cast. Process. Model. Met. Mater., IntechOpen, 2021, https://doi.org/10.5772/intechopen.94392.

[22] M. Riedler, S. Michelic, C. Bernhard, Formation of shrinkage porosity during solidification of steel: numerical simulation and experimental validation, IOP Conf. Ser. Mater. Sci. Eng. 143 (2016) 012035, https://doi.org/10.1088/1757-899X/143/1/012035.

[23] M.A.V. Devanathan, Z. Stachurski, The adsorption and diffusion of electrolytic hydrogen in palladium, Proc. R. Soc. Lond. Ser. Math. Phys. Sci. 270 (1962) 90–102, https://doi.org/10.1098/rspa.1962.0205.

[24] H.L. Frisch, The Time Lag in Diffusion, J. Phys. Chem. 61 (1957) 93–95, https://doi.org/10.1021/j150547a018.

[25] R.M. Barrer, Diffusion in and Through Solids, University Press, 1951 (https://books.google.fr/books?id=sXREAQAAIAAJ).

[26] J.-G. Sezgin, C. Bosch, A. Montouchet, G. Perrin, K. Wolski, Modelling and simulation of hydrogen redistribution in a heterogeneous alloy during the cooling down to 200 °C, Int. J. Hydrog. Energy 42 (2017) 19346–19358, https://doi.org/10.1016/j.ijhydene.2017.03.095.

[27] J.-G. Sezgin, C. Bosch, A. Montouchet, G. Perrin, K. Wolski, Modelling of hydrogen induced pressurization of internal cavities, Int. J. Hydrog. Energy 42 (2017) 15403–15414, https://doi.org/10.1016/j.ijhydene.2017.04.106.

[28] H. Hagi, Y. Hayashi, N. Ohtani, Diffusion Coefficient of Hydrogen in Pure Iron between 230 and 300 K, Trans. Jpn. Inst. Met. 20 (1979) 349–357, https://doi.org/10.2320/matertrans1960.20.349.

[29] O.D. Gonzalez, Measurement of hydrogen permeation in α-iron: analysis of the experiments, Trans. Metall. Soc. AIME 245 (1969) 607–612.